Fatigue crack growth modelling for S355 structural steel considering plasticity-induced crack-closure by means of UniGrow model

Pedrosa, Bruno; Correia, José; Lesiuk, Grzegorz; Rebelo, Carlos; Veljkovic, Milan

DOI
10.1016/j.ijfatigue.2022.107120

Publication date
2022

Document Version
Final published version

Published in
International Journal of Fatigue

International Journal of Fatigue 164 (2022) 107120

Contents lists available at ScienceDirect

International Journal of Fatigue

journal homepage: www.elsevier.com/locate/ijfatigue

Fatigue crack growth modelling for S355 structural steel considering plasticity-induced crack-closure by means of UniGrow model

Bruno Pedrosa [a,*], José Correia [b,c], Grzegorz Lesiuk [d], Carlos Rebelo [a], Milan Veljkovic [c]

[a] University of Coimbra, ISISE, Department of Civil Engineering, Coimbra, Portugal
[b] INEGI & CONSTRUCT, Faculty of Engineering, University of Porto, 4200-465 Porto, Portugal
[c] Faculty of Civil Engineering and Geosciences, Delft University of Technology, 2600 GA Delft, the Netherlands
[d] Wroclaw University of Science and Technology, Department of Mechanics, Materials and Biomedical Engineering, Wrocław, Poland

ARTICLE INFO

Keywords:
Fatigue crack growth
S355
UniGrow model
Crack-closure
Local approaches

ABSTRACT

The UniGrow model is an analytical procedure to assess the fatigue crack growth based on elastic–plastic crack tip stresses and strains. The assumption is that fatigue crack growth (FCG) can be considered as a process of successive crack re-initiations resulting from material damage in the crack tip zone. The main parameters of this model are the crack tip radius and the elementary block size. Experimental FCG data obtained for S355 carbon steel showed that assuming the elementary block size with the same value of the crack tip radius to collapse FCG data using UniGrow model is non-coherent with experimental evidence. In this sense, a new approach is proposed by establish a clear distinction between crack tip radius and elementary block size. The value of the crack tip radius, ρ, was defined by correlation with experimental and numerical values of residual compressive stress field ahead of the crack tip while for the elementary block size, ρ^*, a new expression was proposed which relies on effective stress intensity factor range and cyclic yield strength. This research intends to be a valuable contribution for the implementation of UniGrow model to assess the fatigue crack growth of a material.

1. Introduction

Fatigue crack propagation has been analyzed mainly using the expression proposed by Paris and Erdogan [1]:

$$\frac{da}{dN} = C\left(\Delta K_{appl}\right)^m \tag{1}$$

where da/dN is the fatigue crack growth rate, ΔK_{appl} is the applied value of the stress intensity factor range and C and m are material constants. The main limitation of this model is that mean stress effects are not considered and there are many materials in which the stress ratio changes the FCG behavior. In 1970, Elber [2] studied the influence of mean stress effects on FCG and proposed new parameters to describe it. He introduced the concept of the crack tip closure which conducted to present FCG models based on effective stress intensity factor range, ΔK_{eff}:

$$\frac{da}{dN} = C\left(\Delta K_{eff}\right)^m \tag{2}$$

In 1985, Glinka [3] introduced the use of strain-based fatigue models to analyze FCG process. He developed the concept of discretization using elementary material blocks whose failure defines the crack growth. Later, in 1999 Peeker and Niemi [4] proposed a model for FCG based on the superposition of the near threshold and stable fatigue crack growth regimes using cyclic elastoplastic stress–strain constants as well as strain-life constants. More recently, Noroozi and Glinka [5–7] developed the UniGrow model based on the elastoplastic crack tip stress-stain history analysis in which the influence of the compressive stress field formed ahead of the crack tip during FCG is included. This model was develop using the Smith-Watson-Topper as fatigue damage parameter. In 2007, Hurley and Evans [8] presented a new methodology based on the assumption that the number of cycles to propagate a crack through the cyclic plastic zone is the same as the one to initiate a crack in a specimen under plain strain conditions. In 2017, Ferreira et al [9] proposed the use of strip-yield mechanics to model fatigue crack growth. New developments on crack propagation models based on residual stresses has been proposed by Correia et al. [10], Hafezi et al. [11] and Jesus and Correia [12] which considers the assumption of the UniGrow model but the elastoplastic stress fields are obtained by finite elements. It is also important to refer that the implementation of probabilistic

* Corresponding author.
E-mail address: bruno.pedrosa@uc.pt (B. Pedrosa).

https://doi.org/10.1016/j.ijfatigue.2022.107120
Received 21 March 2022; Received in revised form 27 June 2022; Accepted 3 July 2022
Available online 6 July 2022

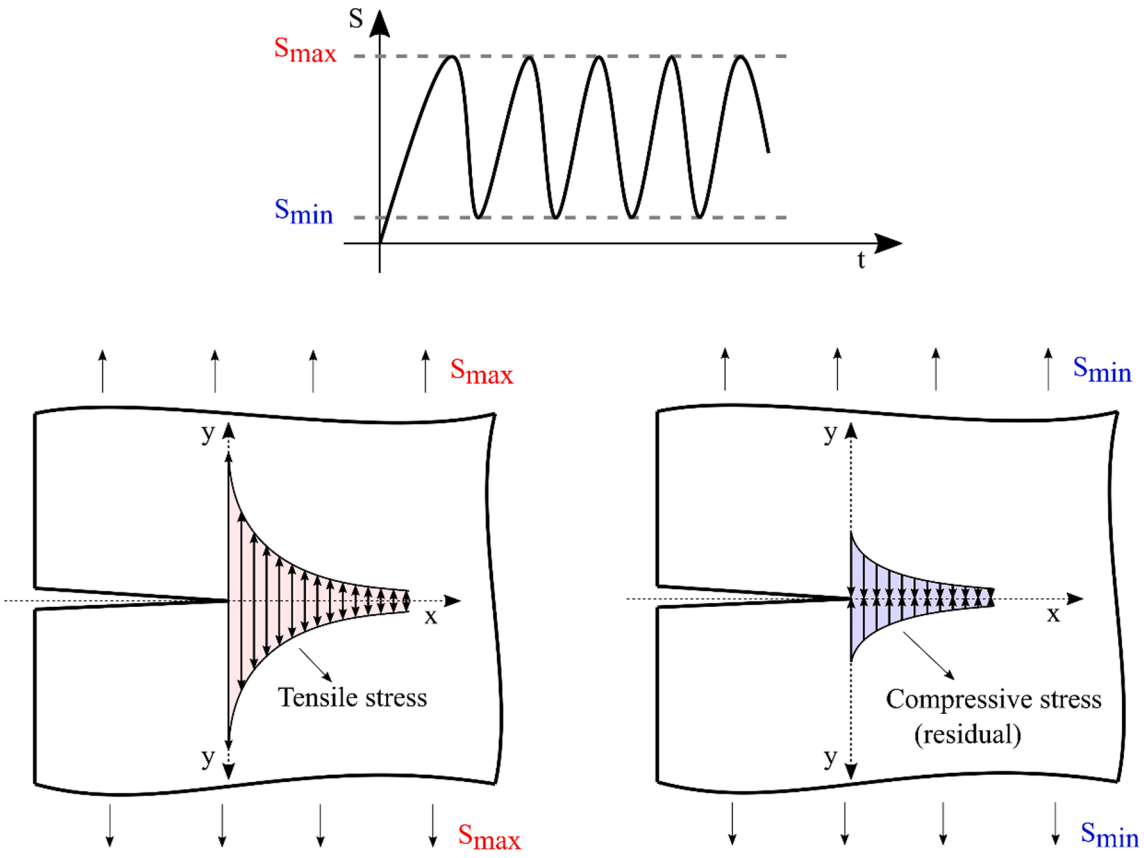

Fig. 1. Schematic representation of remote applied stress and resulting local crack tip stress fields.

analysis to FCG models based on local approaches has been performed by Correia et al. [13] and Bogdanov et al. [14]. These FCG models have been also used in procedures to compute S-N curves of structural details, namely notched plates. Correia et al. [15,16] proposed a general procedure to obtain probabilistic S-N fields for notched plate details.

General applications of UniGrow model are related with FCG for long cracks (>0.5–1.0 mm), however Bang et al [17] proposed a modification on the model for short FCG based on experimental results on aluminum and titanium alloys. Two improvement modelling methods were presented: stress intensity correction and data fitting. Results from both methods were better for high stress levels and stress intensity correction method lead to more accurate predictions. Later on 2019, Bang et al [18] further improved the proposed modifications on the UniGrow model in order to consider both short and long crack growth behavior. More recently, Bang et al [19] developed a unified modelling framework for integrating short and long crack propagation for the formulation of the crack driving force of the UniGrow model.

The stress ratio effects have also been studied by Daniel Kujawski [20–22]. An analytical method to estimate the elastoplastic stress–strain field ahead of the crack tip was proposed and results were compared with experimental and numerical data [20]. Moreover, in 2021 a damaging stress intensity function was proposed (analogous to SWT parameter) to analyze stress ratio effects in metallic materials under constant amplitude loading mainly in threshold and lower Paris region of FCG [21]. Later on 2022, the new crack driving force proposed by Daniel Kujawski [22] was extended to a wide variety of different alloys and for both positive and negative stress ratios.

As it was studied in Mikheevskiy [23], by computing the stresses and strains ahead of the crack tip with a stationary crack, the effect of the prior loading history is neglected. However, it was concluded that it influences only the stresses at maximum load level and insignificant effect on stresses at minimum load level.

In this paper, fatigue crack propagation of S355 is analyzed considering a unified two-stage methodology. This material was chosen because it is commonly used in civil engineering structures that are subjected to fatigue loading conditions, namely bridge structures. Experimental results of low-cycle fatigue tests conducted by different authors are analyzed and a cyclic elastoplastic stress–strain curve is proposed. Fatigue crack growth tests on specimens from S355 were conducted and the applied and effective values of stress intensity factors were measured. The main goal of this scientific investigation was to analyze the implementation of UniGrow model to predict the fatigue crack growth behavior of S355 material. Additionally, it is proposed to distinguish the value of the crack tip radius and the value of the elementary block size. Residual stress intensity factor was computed by means of experimental and numerical procedures which enable to determine the proposed crack tip radius for this material. The elementary block size was considered as dependent on the effective stress intensity factor range and the cyclic yield strength of the material. An expression to compute the elementary block size is proposed that showed good results to collapse FCG experimental data.

2. Fatigue crack propagation model - UniGrow

Fatigue crack growth process is mainly controlled by the stress–-strain field ahead of the crack tip. However, it is not easy to compute elastoplastic stresses and strains at the crack tip since they are strongly dependent on the applied method. To overcome this problem, general approaches to fatigue crack growth are based on fracture mechanics which uses global parameters such as nominal stress, crack length, geometry, for example, which are then combined to obtain one general parameter, usually, the stress intensity factor (SIF). However, the effect of residual stresses induced by reversed plastic deformations affects the correlation between SIF and actual stress–strain field.

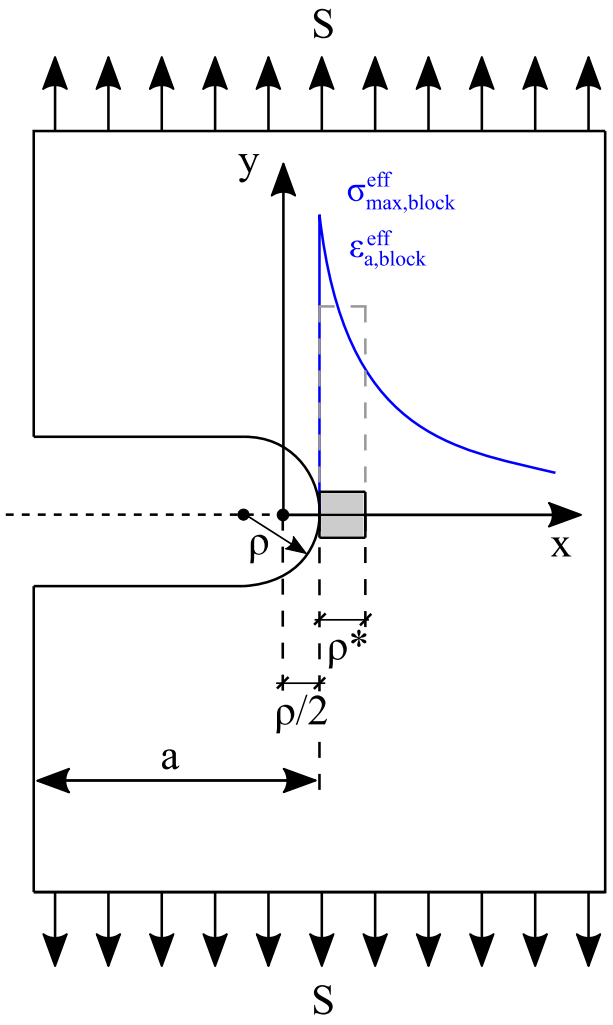

Fig. 2. Schematic representation of the stress and strain distributions ahead of the crack tip induced by a tensile load.

There are several scientific investigations in literature aiming to model the crack on the basis of the mechanics of continuum. Irwin [24] and Hutchinson [25] computed stresses and strains near the crack tip using a sharp crack (tip radius $\rho = 0$) which leads to unrealistically high values. More recently, several authors [3,26] implemented the approach of modelling the crack as a notch with a small but finite tip radius $\rho > 0$. Notch analytical theories are applied and stress–strain field ahead of the crack tip become more realistic. Noroozi et al. [5] suggested that there is a minimum value of the notch tip radius,ρ, that can be considered as a material property and results in the maximum stress concentration which can be generated in the material. Noroozi et al. [5] also emphasizes that the plastic yielding around the crack tip formed during one load reversal generates plastic deformations which resists to be deformed during subsequent reversals of cyclic loading. The effect of plastic deformations ahead of the crack tip can be determined by solving the notched body boundary problem using elastic–plastic material properties resulting in the residual stress field σ_r. Even if nominal stress ratio is positive, a compressive (residual) stress field is generated ahead of the crack tip when the load is at the minimum level as described in Fig. 1. This residual compressive stress field increases as the stress ratio is closer to zero.

Glinka [3] proposes to model the crack with a finite tip radius ρ which allows the calculation of crack tip stress and strain distributions with notch theories and assumes that the crack region just behind the tip remains open – see Fig. 2. The value of ρ stands as the smallest notch tip radius that the material can "feel" as a notch.

Noroozi et al. [5] also suggested that notch tip radius,ρ, can be considered an elementary block size of the material which can be used to discretize the medium of the material in order to determine the relevant stresses and strains ahead of the crack tip. However, it was stated that the elementary block size cannot be associated with any specific microstructural particle size.

The fatigue crack growth model that is implemented in this paper was based on the assumptions presented by Noroozi et al. [5], however the elementary block size, ρ^*, used to compute the relevant stresses and strains ahead of the crack tip was not considered as being the same size of the notch tip radius, ρ. The value of the elementary block size was found by correlation with experimental data and a new formulation is proposed based on the effective stress intensity factor range and on the cyclic yield strength of the material.

The FCG model used in this paper is based on the following assumptions:

- The fatigue crack is analyzed as a notch with a tip radius ρ;
- The Ramberg-Osgood cyclic stress–strain formulation is used to expresses the material behavior;
- The relevant stresses and strains to analyze fatigue crack growth are measured within an elementary block size ρ^* ahead of the crack tip – see Fig. 2. This parameter is a function of the effective stress intensity factor range, ΔK_{eff}, and the cyclic yield strength of the material, σ'_0:

$$\rho^* = \frac{1}{28\pi}\left(\frac{\Delta K_{eff}}{\sigma'_0}\right)^2 \tag{3}$$

- Fatigue crack growth is considered as successive crack re-initiations over the distance ρ^*;
- The number of cycles N to reach failure of the first elementary block ahead of the crack tip can be determined using the Smith-Watson-Topper (SWT) fatigue damage parameter:

$$D_{block} = \sigma^{eff}_{max,block}\varepsilon^{eff}_{a,block} \tag{4}$$

where D_{block} is the fatigue damage of the block, $\sigma^{eff}_{max,block}$ corresponds to the maximum effective stresses over the block size and $\varepsilon^{eff}_{a,block}$ is the effective strain amplitude over the block size.

- The fatigue crack growth rate is determined as the average fatigue crack growth rate over the elementary block size, ρ^*:

$$\frac{da}{dN} = \frac{\rho^*}{N_{Block}} \tag{5}$$

where N_{Block} is the number of cycles to fail the elementary block.

2.1. Stresses and strains at the crack tip

The Neuber rule [27] is used to compute the elastoplastic stresses and strains ahead of the crack tip in which linear elastic values are used as input data. In the following subsections, the analysis is made only for the case of tensile loading ($R_\sigma > 0$).

2.1.1. Linear elastic analysis

Linear elastic stress field is computed using the concept of linear elastic fracture mechanics (LEFM) by assuming a notch with tip radius ρ and crack length a. The Creager-Paris solution [28] was used and the result is presented in Eq. (6).

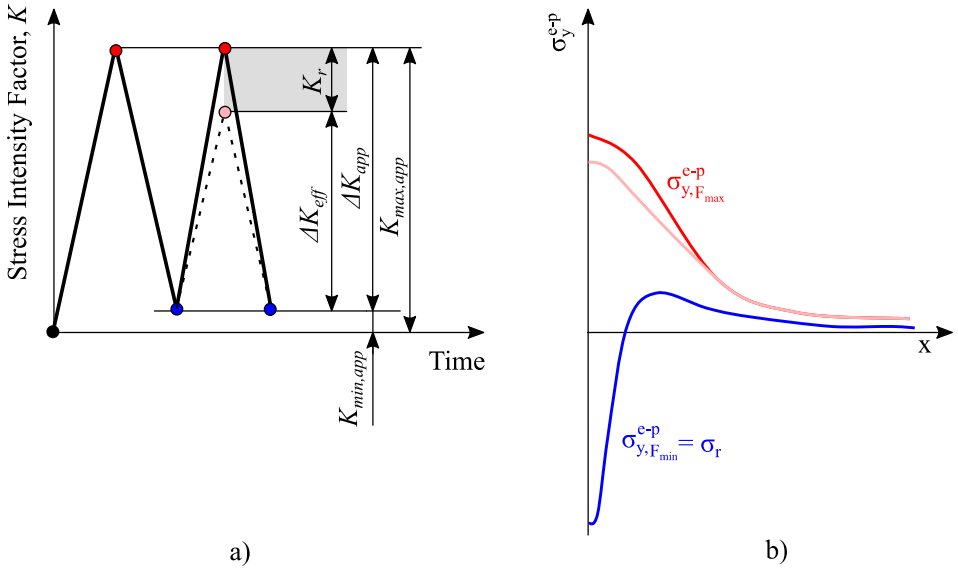

Fig. 3. a) Schematic representation of stress intensity factor history; b) elastic–plastic stress field induced by cyclic loading ahead of the crack tip.

$$\begin{cases} \sigma_x^e = \dfrac{K}{\sqrt{2\pi x}}\left(1-\dfrac{\rho}{2x}\right) \\ \sigma_y^e = \dfrac{K}{\sqrt{2\pi x}}\left(1+\dfrac{\rho}{2x}\right) \\ \tau_{xy}^e = 0 \end{cases} \tag{6}$$

With these equations, the elastic stress–strain field ahead of the crack tip is fully characterized. Variables σ_x^e and σ_y^e are the elastic normal stresses (directions according to Fig. 2), τ_{xy}^e is the elastic shear stress component and K is the stress intensity factor.

2.1.2. Elastoplastic analysis

Elastoplastic stress–strain analysis is used to determine the actual stress–strain ahead of the crack tip. This is accomplished using the Neuber rule which uses the equivalence of strain energy density at the notch tip between the hypothetical linear-elastic notch tip stress–strain input data and the actual elastic–plastic response. This approach was originally derived for a uniaxial stress state, but recently Moftakhar et al. [29] extended it for multi-axial proportional and non-proportional loading conditions. In cases of elements in plane strain, the near tip stress–strain field is tri-axial but the third principal stress is a function of the other two. Additionally, the components of the elastic stress tensor change proportionally during loading which means that Hencky equations of the theory of plasticity can be used. In this sense, the whole notch-tip stress–strain problem can be reduced to the solution of a set of five nonlinear algebraic equations including Hencky stress–strain relationships, Ramberg-Osgood equation and multi-axial Neuber rule:

A) Generalized Neuber rule.

$$\sigma_y^e\varepsilon_y^e + \sigma_x^e\varepsilon_x^e = \sigma_y^{e-p}\varepsilon_y^{e-p} + \sigma_x^{e-p}\varepsilon_x^{e-p} \tag{7}$$

B) Constitutive stress–strain relationships.

$$\varepsilon_z^{e-p} = -\frac{\nu}{E}\left(\sigma_y^{e-p}+\sigma_x^{e-p}\right) - \frac{f\left(\sigma_{eq}^{e-p}\right)}{2\sigma_{eq}^{e-p}}\left(\sigma_y^{e-p}+\sigma_x^{e-p}\right) \tag{8}$$

$$\varepsilon_y^{e-p} = \frac{1}{E}\left(\sigma_y^{e-p}-\nu\sigma_x^{e-p}\right) + \frac{f\left(\sigma_{eq}^{e-p}\right)}{2\sigma_{eq}^{e-p}}\left(\sigma_y^{e-p}-0.5\sigma_x^{e-p}\right) \tag{9}$$

$$\varepsilon_x^{e-p} = \frac{1}{E}\left(\sigma_x^{e-p}-\nu\sigma_y^{e-p}\right) + \frac{f\left(\sigma_{eq}^{e-p}\right)}{2\sigma_{eq}^{e-p}}\left(\sigma_x^{e-p}-0.5\sigma_y^{e-p}\right) \tag{10}$$

Where

$$\sigma_{eq}^{e-p} = \sqrt{\left(\sigma_y^{e-p}\right)^2 - \sigma_y^{e-p}\sigma_x^{e-p} + \left(\sigma_x^{e-p}\right)^2} \tag{11}$$

$$f\left(\sigma_{eq}^{e-p}\right) = \left(\frac{\sigma_{eq}^{e-p}}{K'}\right)^{\frac{1}{n'}} \tag{12}$$

C) The fractional contribution of the total strain energy density.

$$\frac{\sigma_y^e\varepsilon_y^e}{\sigma_y^e\varepsilon_y^e + \sigma_x^e\varepsilon_x^e} = \frac{\sigma_y^{e-p}\varepsilon_y^{e-p}}{\sigma_y^{e-p}\varepsilon_y^{e-p} + \sigma_x^{e-p}\varepsilon_x^{e-p}} \tag{13}$$

In these set of equations σ_x^e, σ_y^e and ε_x^e, ε_y^e and ε_z^e are the elastic normal stresses and strains, respectively, and σ_x^{e-p}, σ_y^{e-p} and ε_x^{e-p}, ε_y^{e-p} and ε_z^{e-p} are the elastoplastic normal stresses and strains, respectively (directions according to Fig. 2). Additionally, ν corresponds to the Poisson coefficient, E is the Young's modulus, K' is the cyclic strain hardening coefficient and n' is the cyclic strain hardening exponent.

2.2. Effective stress intensity factor

The set of equations presented before enable the computation of the stress–strain field ahead of the crack tip induced by a load reversal which can be represented by the fluctuations of the stress intensity factor, ΔK_{app} – see Fig. 3a). The analysis and computation of residual stress field, $\sigma_r(x)$, formed ahead of the crack tip by the load reversal is then executed. Fig. 3b) represents a schematic distribution of stresses ahead of the crack tip corresponding to maximum and minimum applied load level for positive (but close to zero) value of stress ratio. In this situation, a compressive residual stress field is generated at minimum load level whose effects need to be included in the analysis. In this sense, an effective stress intensity factor range is computed by deduct the residual values of the stress intensity factor on the applied values of the stress intensity factors.

$$K_r = \int_0^a \sigma_r(x)m(x,a)dx \tag{14}$$

The physical crack tip location at '$x = a$' was chosen as the upper

Table 1
Experimental results from LCF tests on smooth S355 specimens.

Source	ε_a[%]	ε_a^E[%]	ε_a^P[%]	σ_a[MPa]	σ_{max}[MPa]	2 N_f
Carvalho [31]	1.000	0.235	0.765	419.6	420.4	882
	1.000	0.235	0.765	428.6	429.6	798
	0.500	0.200	0.300	365.7	367.7	5 684
	0.500	0.190	0.310	371.2	373.5	6 282
	0.750	0.175	0.200	342.2	344.9	21 840
	0.750	0.175	0.200	336.7	336.8	15 606
	0.250	0.145	0.105	292.0	293.4	73 208
	0.250	0.150	0.100	292.0	292.2	56 504
	0.200	0.130	0.070	284.2	287.9	29 912
	0.200	0.135	0.065	272.3	273.5	79 152
	0.150	0.120	0.030	261.7	280.2	162 036
	0.125	0.115	0.010	240.7	245.8	2 777 354
Jesus et al. [30]	1.000	0.279	0.722	487.7	497.4	672
	1.000	0.287	0.714	484.1	482.4	1 084
	0.500	0.215	0.285	408.7	409.5	9 610
	0.500	0.182	0.319	331.8	329.8	4 018
	0.250	0.141	0.110	284.8	282.9	32 350
	0.200	0.154	0.047	307.7	311.1	59 002
	0.200	0.164	0.036	330.6	376.5	128 488
	0.175	0.150	0.026	290.8	292.7	556 486
	0.150	0.140	0.011	268.2	253.3	1 722 608

Table 2
Cyclic elastoplastic and fatigue properties of S355.

E [GPa]	K' [MPa]	n' [-]	σ'_0 [MPa]	σ'_f [MPa]	b [-]	ε'_f [-]	c [-]
210	804.6	0.132	180.2	1058.8	−0.110	0.287	−0.542

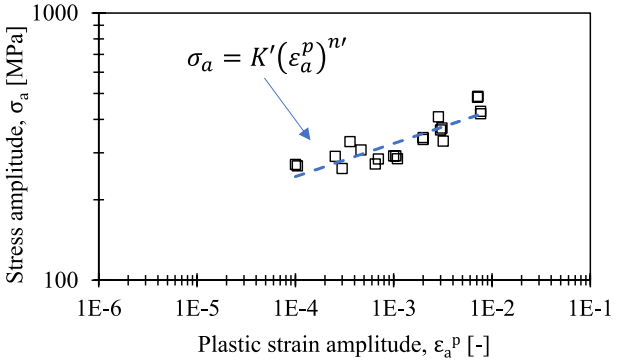

Fig. 4. Determination of strain hardening coefficient and exponent for S355 material.

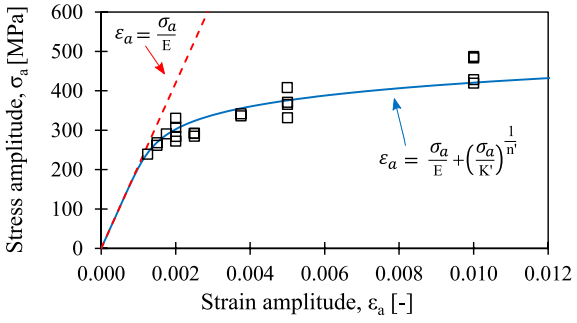

Fig. 5. Stress–strain cyclic curve for S355 material.

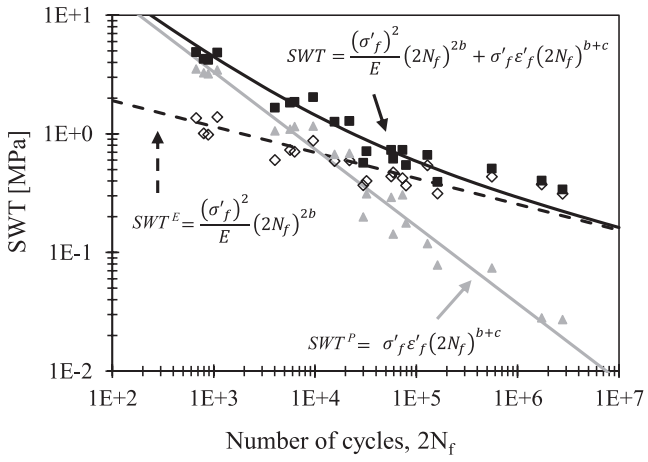

Fig. 6. SWT-life data for S355 and its elastic and plastic components.

limit of the integration. The universal weight function expression for CT specimens (Eq. (15)) was used in the analysis.

$$m(x,a) = \frac{2}{\sqrt{2\pi(a-x)}}\left[1 + M_1\left(1-\frac{x}{a}\right)^{1/2} + M_2\left(1-\frac{x}{a}\right)^{1} + M_3\left(1-\frac{x}{a}\right)^{3/2}\right] \quad (15)$$

The geometry dependent factors M_1, M_2 and M_3 for a CT specimen are given in Glinka [5]. The effective values of the stress intensity factor to use in fatigue crack growth analysis are based on the applied values of the stress intensity factor affected by the residual value of the stress intensity factor. Its influence is considered by changing (decreasing) the maximum value of the stress intensity factor. The minimum value remains equal to the applied value. The effective value of the stress intensity factor range, ΔK_{eff}, and the effective value of the maximum stress intensity factor, $K_{max,eff}$, are presented in Eq. (16) and Eq. (17), respectively. Since the residual stress intensity factor is computed from compressive stresses, its value is negative.

$$\Delta K_{eff} = \Delta K_{app} + K_r \quad (16)$$

$$K_{max,eff} = K_{max,app} + K_r \quad (17)$$

3. Experimental characterization

3.1. Low cycle fatigue

There are a set of experimental results on literature related to the characterization of cyclic elastoplastic behaviour of S355, namely the experimental campaign performed by Jesus et al. [30] and Carvalho [31]. They conducted low cycle fatigue (LCF) tests on smooth specimens according to ASTM E606 [32] under strain controlled conditions. The strain ratio was set to −1 and the strain rate to 0.8%/s. The stabilized cyclic stress–strain curve was used to compute elastic and plastic strain amplitudes and results are summarized in Table 1. A representative cyclic stress–strain curve of the material was defined using the Ramberg-Osgood expression described in Eq. (18) which relates strain amplitude, ε_a, and stress amplitude, σ_a. Elastic and plastic strain amplitudes are identified as ε_a^E and ε_a^P, respectively. The obtained values of the strain hardening coefficient K' and the strain hardening exponent n' are presented in Table 2 considering the linear regression presented in Fig. 4.

$$\varepsilon_a = \varepsilon_a^E + \varepsilon_a^P = \frac{\sigma_a}{E} + \left(\frac{\sigma_a}{K'}\right)^{1/n'} \quad (18)$$

The elastic and elastic–plastic stress–strain cyclic curve was computed and results are presented in Fig. 5. This representation allowed to determine the cyclic yield strength of the material, σ'_0, whose value is presented in Table 2.

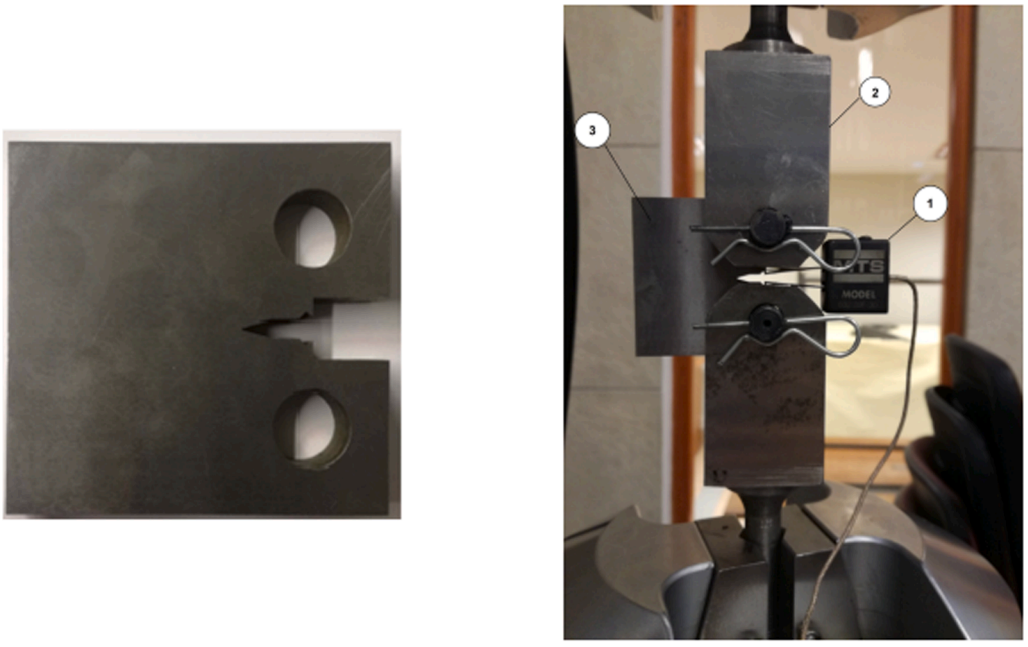

Fig. 7. a) CT specimen made from S355. b) Apparatus of FCG test: 1-MTS clip gage (extensometer); 2-MTS clevis grip for fracture mechanics; 3-specimen.

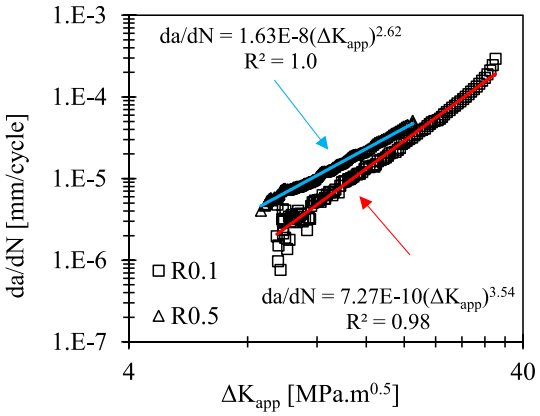

Fig. 8. Fatigue crack growth rate for S355: applied values.

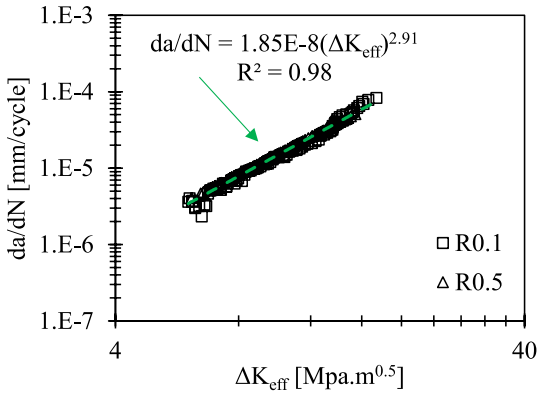

Fig. 10. Fatigue crack growth rate for S355: effective values.

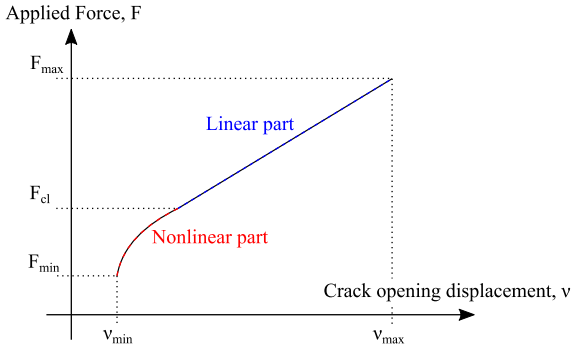

Fig. 9. Determination of crack closure force in a load cycle.

Using the stabilized cyclic stress–strain curve for each experimental test, it is possible to compute the elastic and plastic strain amplitudes. Cyclic elastoplastic data is correlated with number of cycles at failure

Table 3
Summary of fatigue crack propagation parameters for S355.

		C*	m
ΔK_{app}	$R_\sigma = 0.1$	7.27E-10	3.54
	$R_\sigma = 0.5$	1.63E-8	2.62
ΔK_{eff}		1.85E-8	2.91

* da/dN in mm/cycle and ΔK in [MPa.m$^{0.5}$].

Table 4
Estimation of crack tip radius: comparison with experimental results using MSE.

ρ[m]	7.4E-6	5.4E-6	3.4E-6
	MSE	MSE	MSE
$R_\sigma = 0.1$	0.60	0.43	0.26
$R_\sigma = 0.5$	0.72	0.57	0.40

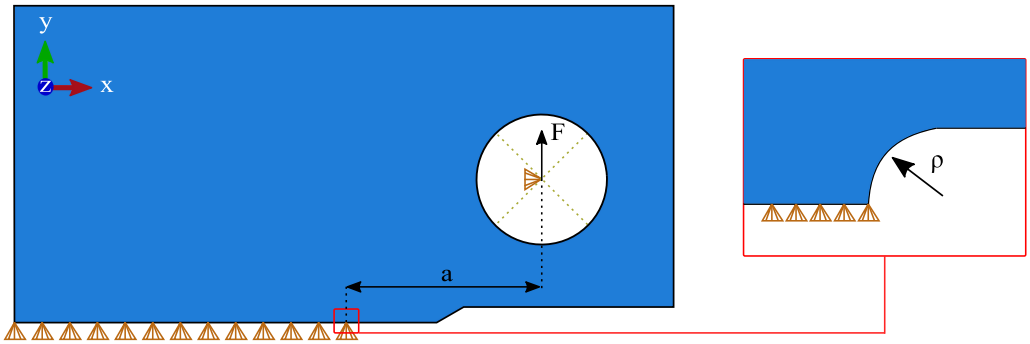

Fig. 11. Boundary conditions and load definitions of the numerical model to compute residual stresses ahead of the crack tip.

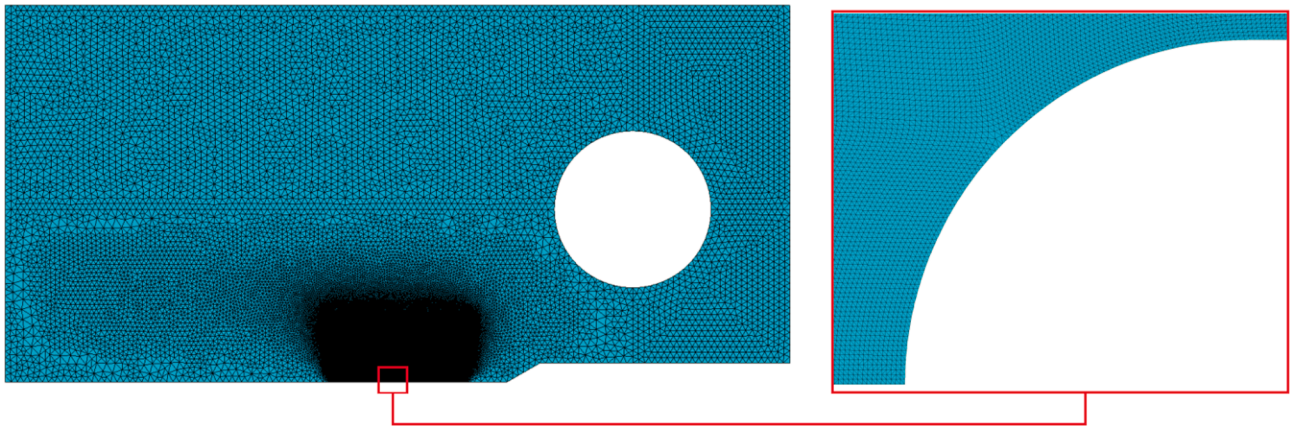

Fig. 12. Finite element mesh of the numerical model.

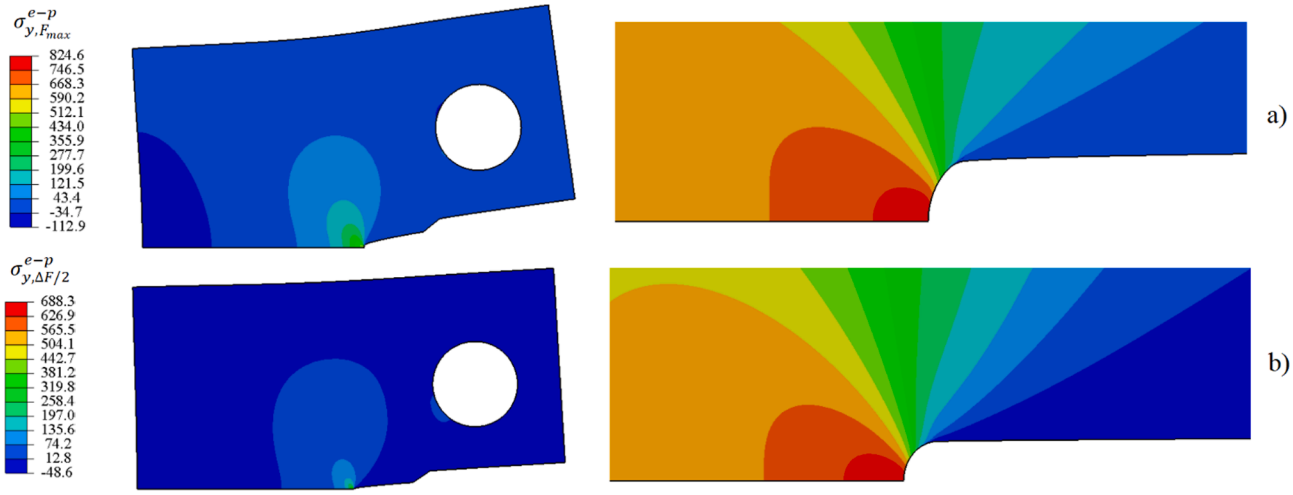

Fig. 13. Elastoplastic stress field (in MPa) for crack length $a = 18.67mm$ and $R_\sigma = 0.1$: a) at maximum load $F = F_{max}$; b) at half of range load value $F = \Delta F/2$.

using the Smith, Watson and Topper (SWT) model [33] which considers mean stress effects. It correlates fatigue life N_f with the product of the maximum stress σ_{max} and strain amplitude ε_a as described in the following equation.

$$\varepsilon_a \sigma_{max} = \frac{(\sigma'_f)^2}{E}(2N_f)^{2b} + \sigma'_f \varepsilon'_f (2N_f)^{b+c} \tag{19}$$

Elastic component is expressed by the fatigue strength coefficient σ'_f and fatigue strength exponent b while the plastic component is expressed by the fatigue ductility coefficient ε'_f and fatigue ductility exponent c. These parameters were determined using a linear regression analysis on the experimental data from elastic and plastic components. Fig. 6 presents the obtained curve for elastic and plastic SWT-life components as well as total SWT-life. The obtained values for these parameters are presented in Table 2.

3.2. Fatigue crack growth rate

Crack propagation tests were performed using CT specimens in accordance with the procedure of ASTM E647 [34] under load controlled conditions. Fig. 7 presents specimens produced for this

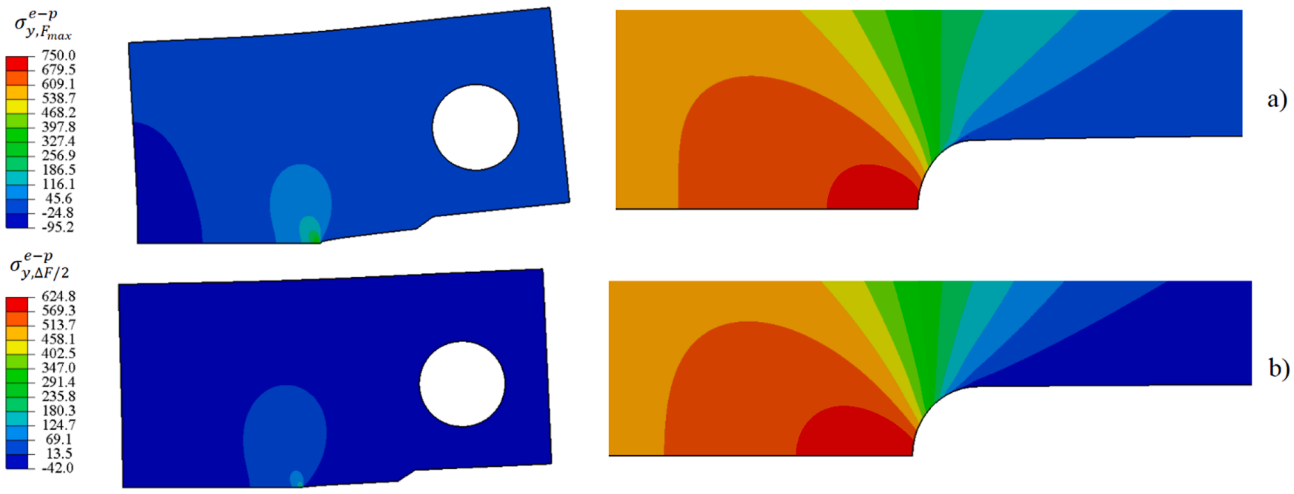

Fig. 14. Elastoplastic stress field (in MPa) for crack length $a = 23.92mm$ and $R_\sigma = 0.1$: a) at maximum load $F = F_{max}$; b) at half of range load value $F = \Delta F/2$.

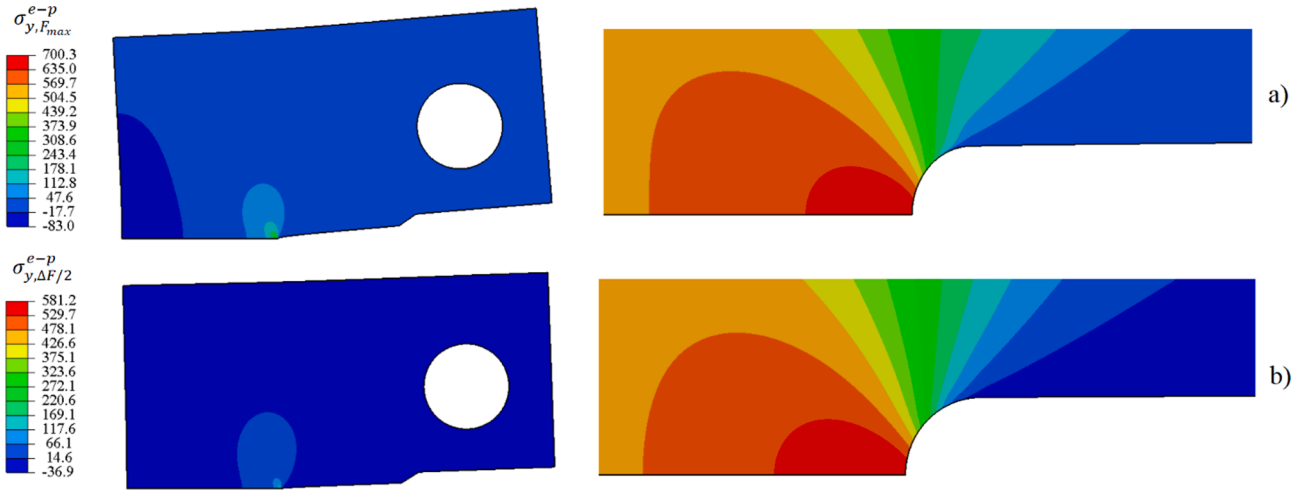

Fig. 15. Elastoplastic stress field (in MPa) for crack length $a = 27.64mm$ and $R_\sigma = 0.1$: a) at maximum load $F = F_{max}$; b) at half of range load value $F = \Delta F/2$.

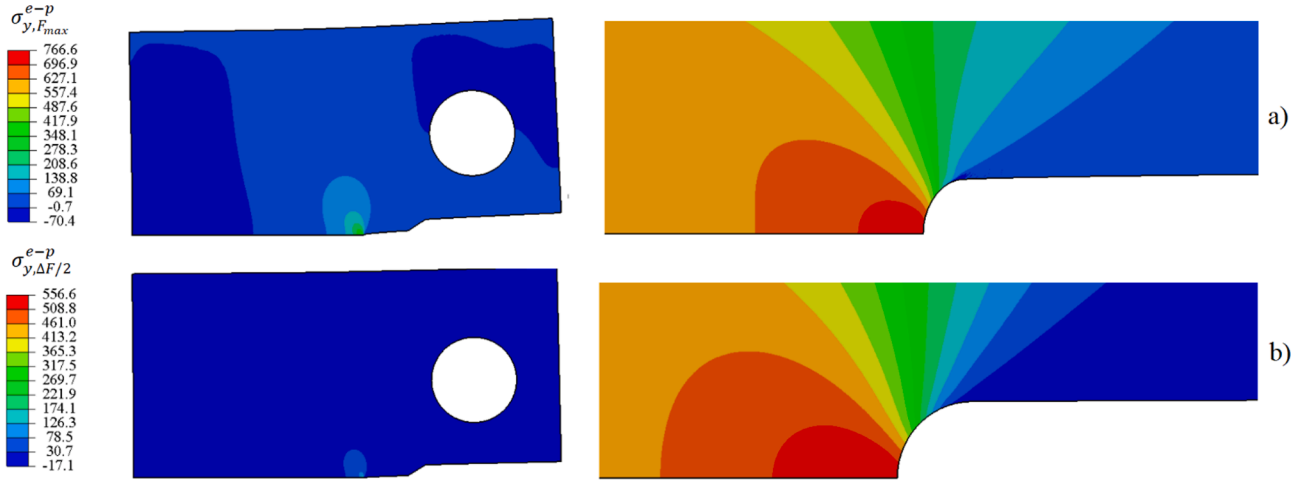

Fig. 16. Elastoplastic stress field (in MPa) for crack length $a = 16.53mm$ and $R_\sigma = 0.5$: a) at maximum load $F = F_{max}$; b) at half of range load value $F = \Delta F/2$.

experimental campaign defined by W (width) = 50 mm and B (thickness) = 12 mm. One specimen was tested under stress ratio $R_\sigma = 0.1$ and controlled by ΔK decreasing procedure and one specimen was tested under stress ratio $R_\sigma = 0.5$ and controlled by ΔF constant procedure. Frequency was set to 12 Hz. A fatigue pre-crack was prepared on the specimen as recommended in the standard using a ΔK not higher than 13–15 MPa.m$^{0.5}$.

The applied force F and the crack opening displacement (COD) ν

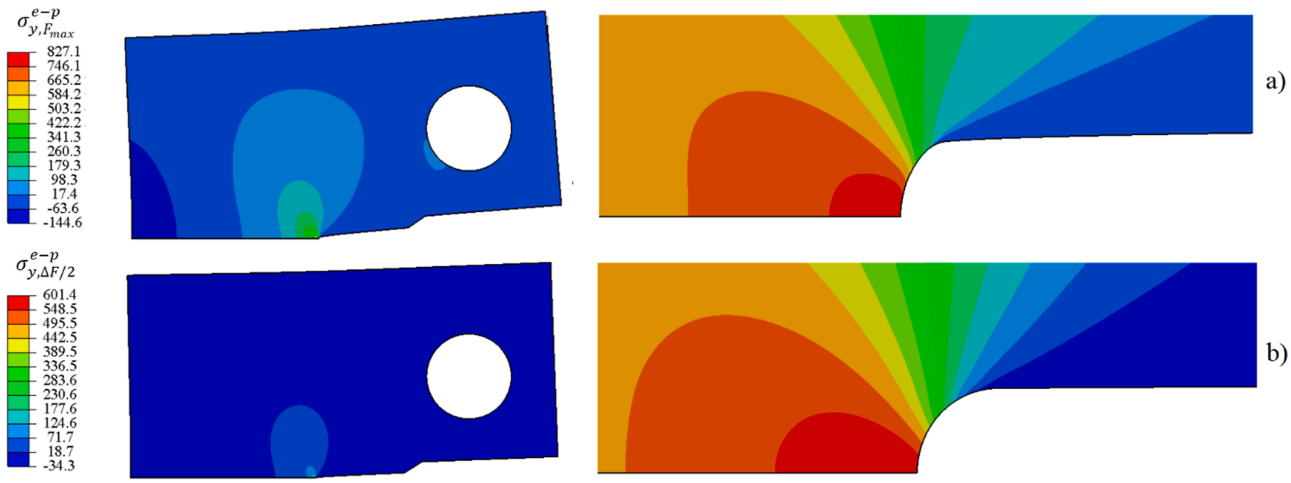

Fig. 17. Elastoplastic stress field (in MPa) for crack length $a = 23.12mm$ and $R_\sigma = 0.5$: a) at maximum load $F = F_{max}$; b) at half of range load value $F = \Delta F/2$.

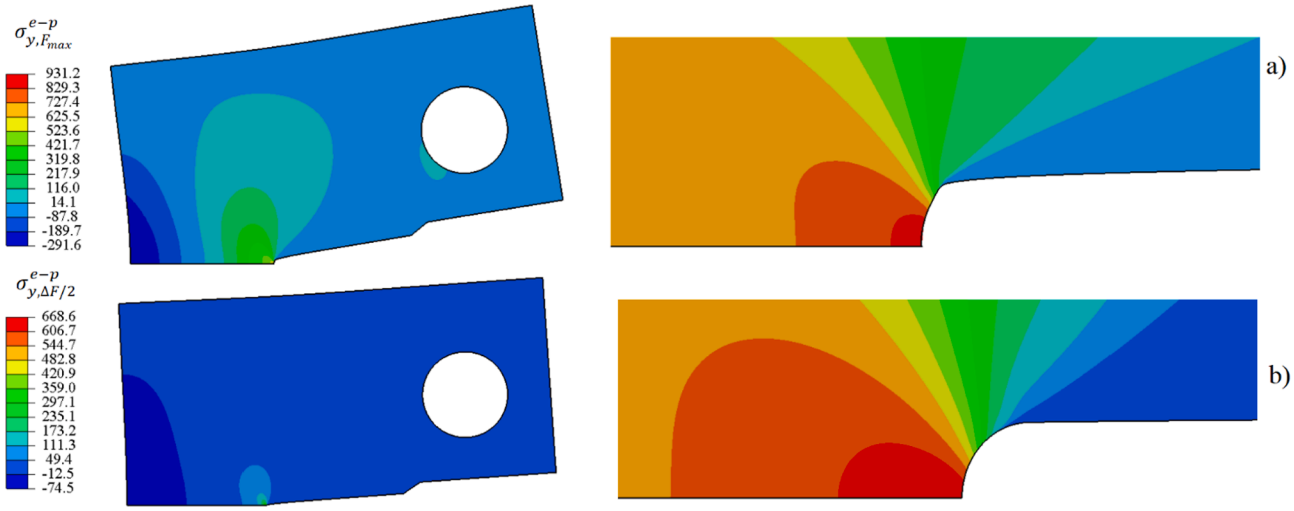

Fig. 18. Elastoplastic stress field (in MPa) for crack length $a = 29.98mm$ and $R_\sigma = 0.5$: a) at maximum load $F = F_{max}$; b) at half of range load value $F = \Delta F/2$.

were monitored during the test which is then used to compute the crack length using compliance method, a, and the applied stress intensity factor ranges by applying the compliance method described in ASTM E647 [34]:

$$\Delta K_{app} = \frac{\Delta F}{B\sqrt{W}} \frac{(2+\alpha)}{(1-\alpha)^{3/2}} \left(0.886 + 4.64\alpha - 13.32\alpha^2 + 14.72\alpha^3 - 5.6\alpha^4\right) \tag{20}$$

in which α is the ratio a/W.

Fig. 8 presents the experimental results relating fatigue crack growth rates with applied stress intensity factor ranges. It is evident that this material is influenced by the stress ratio. Lower stress ratio led to smaller fatigue crack growth rates. The slope of the regression line for stress ratio equal to 0.1 is superior to the slope of the regression line for stress ratio equal to 0.5 leading to reduced fatigue crack growth rates for smaller values of applied stress intensity factors ranges which means that mean stress effects are more relevant in this region.

During the experimental test, for each chosen cycle, at least two hysteresis loops were registered in order to compute the F-ν behaviour. The effective stress intensity factor range, ΔK_{eff}, was determined using the Elber concept [2] by computing at crack closure point the force, F_{cl}, which consists of splitting the recorded F-ν curve into linear and nonlinear segments. This approach is described in Fig. 9.

The linear and nonlinear components of the curve are described using Eq. (21) and Eq. (22), respectively.

$$\nu_L = A_0 + A_1 F \tag{21}$$

$$\nu_Q = B_0 + B_1 F + B_2 F^2 \tag{22}$$

Coefficients A_0 and A_1 are determined by linear regression method, while B_0, B_1 and B_2 were obtained with the following conditions:

$$\nu_L = \nu_Q \tag{23}$$

$$\frac{d(\nu_Q)}{dF} = \frac{d(\nu_L)}{dF}, for F = F_{cl} \tag{24}$$

In this case, B_0, B_1 and B_2 should be optimal from the mathematical point of view which can be found by minimizing the value of the residual sum of squares (RSS).

$$\xi = \frac{1}{(\nu_{max} - \nu_{min})^2} \sum_{i=1}^{N} \left(\frac{(\nu_Q - \nu_i)^2, for F_i < F_{cl}}{(\nu_Q - \nu_i)^2, for F_i \geq F_{cl}} \right) \tag{25}$$

Parameters ν_{max} and ν_{min} are the extreme values of COD for every cycle. This approach can be easily used in automated experiments, however data can be influenced by large degree of noise or wrong tuning. The effective stress intensity factor range can then be calculated using the Elber closure function as:

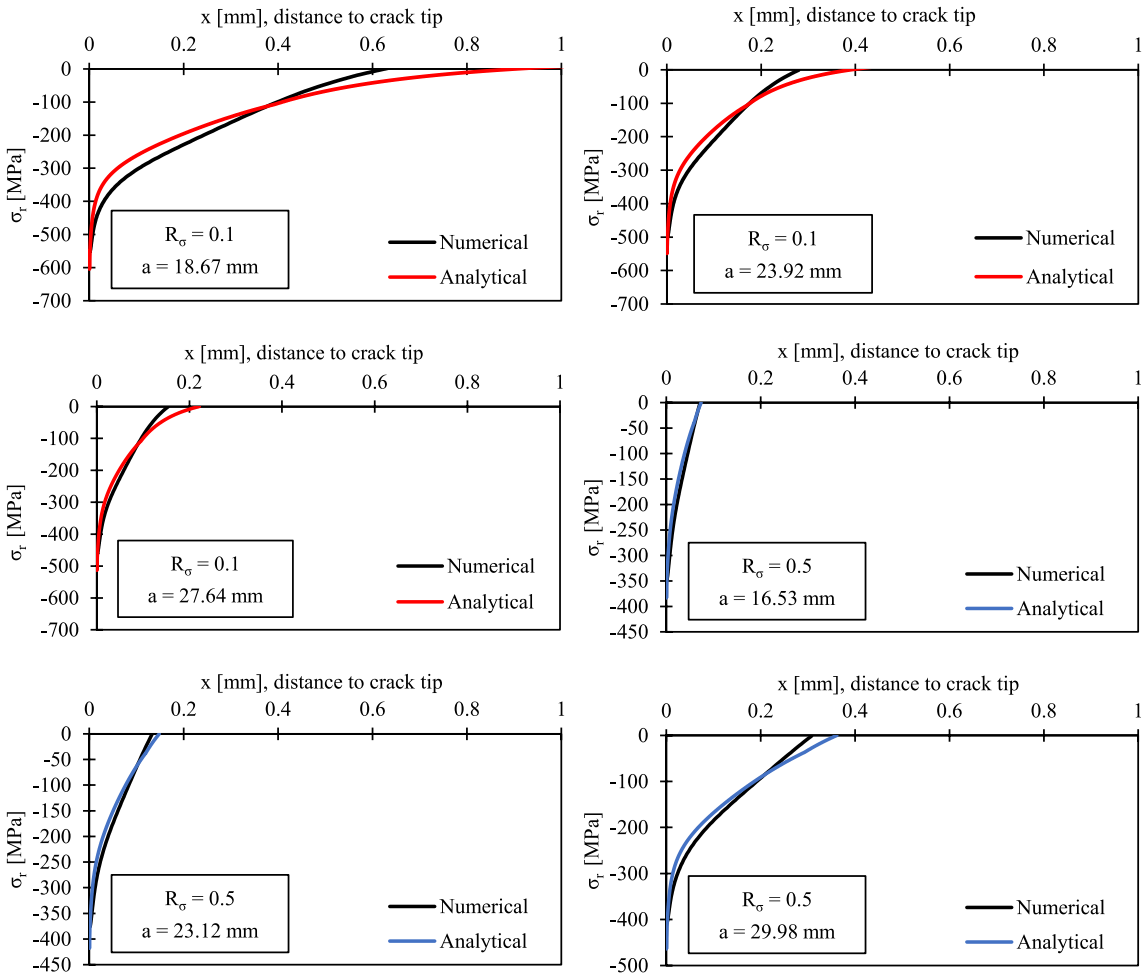

Fig. 19. Residual compressive stresses ahead of the crack tip induced by reversed cyclic plasticity.

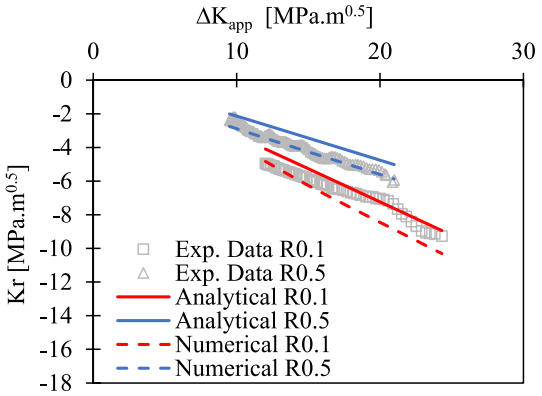

Fig. 20. Residual stress intensity factor for different values of applied stress intensity factor ranges.

$$\Delta K_{eff} = \frac{F_{max} - F_{cl}}{F_{max} - F_{min}} \Delta K_{app} \tag{26}$$

where $F_{\max(min)}$ represents the maximum (and minimum) force in each cycle of loading, F_{cl} is the crack closure load force obtained from hysteresis loop analysis. Experimental results for effective fatigue crack growth are presented in Fig. 10. Data converged to a uniform linear performance. A summary of results is presented in Table 3.

4. Residual stress intensity factor

The UniGrow analytical procedure described in Section 2 to compute residual stresses was implemented. The main parameter that influences residual stresses is the crack tip radius, ρ. The criterion chosen to define the correct value of the crack tip radius was by minimizing the mean squared error (MSE) when analytical values of residual stress intensity factors are compared to experimental values. Eq. (27) presents how MSE is computed using $K_{r,i}$ as the experimental value and $\widehat{K}_{r,i}$ as the estimation value of the residual stress intensity factor. It was found that the size of the tip radius that lead to good correlation with experimental results for both stress ratios is $\rho = 3.4E^{-6}m$ since the value of MSE is inferior to 0.5 for both values of stress ratio as it is possible to observe in Table 4. The comparison between experimental and analytical stress intensity factor values is also presented in Fig. 20. The value found in this paper for crack tip radius differs from the value proposed in Correia et al. [13] ($\rho = 5.5E^{-5}m$) but it can be explained by the fact that their approach was based only on numerical and analytical values of residual stress intensity factor and in the present research we have experimental values to validate this parameter.

$$MSE = \frac{1}{n}\sum_{i=1}^{n}\left(K_{r,i} - \widehat{K}_{r,i}\right)^2 \tag{27}$$

The analytical procedure enabled to compute residual stresses ahead of the crack tip that result from reversal plastification. The value of the crack tip radius, $\rho = 3.4E^{-6}m$, was then used to create a numerical model based on finite elements as presented in Fig. 11 using Abaqus

Table 5
Residual stress intensity factor obtained by three different methods.

				$R_\sigma = 0.1$					
a[mm]	18.67			23.92			27.64		
K_r [MPa.m$^{0.5}$]	Exp. −9.3	Ana. −8.9	Num. −10.3	Exp. −6.2	Ana. −5.6	Num. −6.7	Exp. −4.9	Ana. −4.1	Num. −4.8
				$R_\sigma = 0.5$					
a[mm]	16.53			23.12			29.98		
K_r [MPa.m$^{0.5}$]	Exp. −2.4	Ana. −2.0	Num. −2.8	Exp. −3.7	Ana. −3.0	Num. −3.9	Exp. −5.9	Ana. −5.0	Num. −5.87

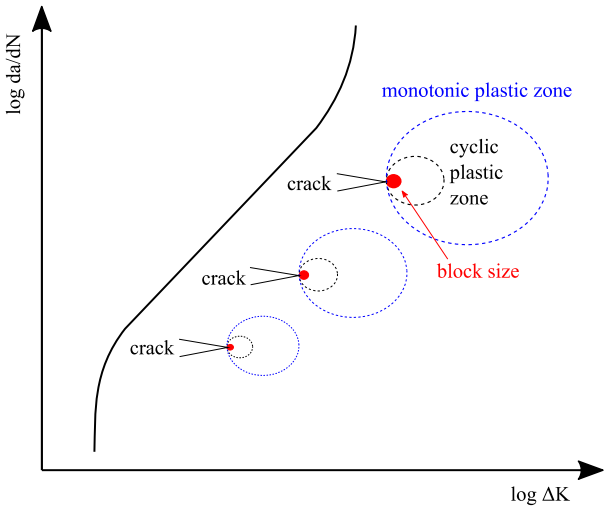

Fig. 21. Schematic illustration of monotonic and cyclic plastic zone and block size during FCG test.

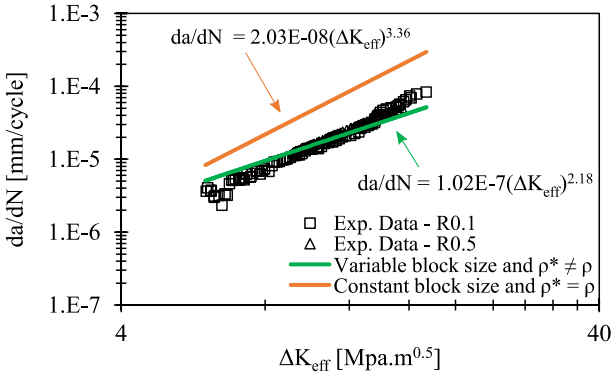

Fig. 22. Comparison between analytical and experimental values of effective fatigue crack growth rates.

software [35].

Taking the advantage of the symmetry plan, the geometry of the CT specimen was defined considering the experimental tests. Three analysis were performed for each value of R_σ varying the value of the crack length, a. The material model implemented in this numerical analysis follows the values obtained for the cyclic elastoplastic behaviour of S355 presented in Table 2. Boundary conditions of the numerical model are Uy = URx = URz = 0 in the symmetry line and Ux = 0 in the hole of the loading pin. Finite element mesh is presented in Fig. 12 and it is composed of CPS3 two-dimensional elements (3-node linear plane stress triangle). The geometric discontinuity in the crack tip requires a refined mesh to get accurate values of stresses and strains, therefore the envelope of this zone has a mesh size smaller than the mesh size in the model and the minimum size in this zone is 4.6E-5 mm.

These numerical analyses enable to get the stress field ahead of the crack tip aiming to compute compressive (residual) stresses and then residual stress intensity factor. From Figs. 13–18 it is possible to observe the stress field at maximum applied load and at half of the applied load range for three models with stress ratio equal to 0.1 and for three models with stress ratio equal to 0.5 varying the crack length. Residual stresses generated from each load reversal were computed considering the stress field ahead of the crack tip at maximum applied load minus two times the stress field ahead of the crack tip at half of the applied load range as presented in the following equation. The value of the applied load was taken from experimental data.

$$\sigma_r = \sigma^{e-p}_{y,F_{max}} - 2 \bullet \sigma^{e-p}_{y,\Delta F/2} \tag{28}$$

The comparison between Unigrow analytical procedure and numerical approach to compute residual stress field ahead of the crack tip is presented in Fig. 19. The internal (residual) stresses induced by the reversed cyclic plasticity is shown for three different values of crack length for each stress ratio. It is possible to observe a very good correlation between analytical and numerical results.

The compressive residual stresses ahead of the crack tip were then used to compute the residual stress intensity factor, K_r, using in integration method presented in Eq. (14). Table 5 presents the results for the three values of crack length selected for each value of stress ratio comparing the results for experimental, analytical and numerical approach. It is possible to observe a very good correlation between both analytical and numerical approaches to experimental results.

The relation between residual stress intensity factor and the applied stress intensity factor range is presented in Fig. 20. Higher values of applied stress intensity factor range conducted to higher values of

Table 6
Analytical results to compute fatigue crack propagation rate based on effective stress intensity factor range.

ΔK_{eff} [MPa.m$^{0.5}$]	Variable block size and $\rho^* \neq \rho$				Constant block size and $\rho^* = \rho$			
	Block size, ρ^* [m]	SWT [-]	$2N_f$ [-]	da/dN [mm/cycle]	Block size,ρ^* [m]	SWT [-]	$2N_f$ [-]	da/dN [mm/cycle]
7.1	1.7E-05	2.01	4809	7.3E-06		6.7	477	1.4E-05
9.8	3.4E-05	2.05	4614	1.5E-05	3.4E-6	12.8	157	4.3E-05
15.0	7.9E-05	2.15	4203	3.8E-05		30.5	37	1.8E-04

residual stress intensity factor. It is also evident that residual stress intensity factor is smaller for higher values of stress ratio. It is also possible to observe the good correlation between analytical and numerical approaches with experimental results for all values of applied stress intensity factor range.

5. Fatigue crack growth rates

Using the values for the effective stress intensity factor range computed for the three crack length values for both $R_\sigma = 0.1$ and $R_\sigma = 0.5$, fatigue crack growth rates were evaluated by means of UniGrow analytical approach described in Section 2. The original UniGrow model assumes that the elementary block size used to collapse FCG data is the same as the crack tip radius. This approach neglects the effect of the increasing plastic zone ahead of the crack tip during FCG test with constant stress ratio as represented in Fig. 21. In order to consider this effect, the elementary block size, ρ*, used in this investigation to collapse FCG data is based on a similar relation used to obtain the crack tip plasticity radius. As it is described in Eq. (3), the proposed expression relies on the effective stress intensity factor, ΔK_{eff}, and on the cyclic yield strength of the material, σ'_0 and it was defined by correlation with experimental data.

In order to compare the original procedure of UniGrow model and the proposed method, the fatigue crack growth data and the stress intensity factor range obtained experimentally is compared with predicted values in Fig. 22. In the original procedure, the elementary block size used to collapse the FCG data has the same value of the crack tip radius implemented to compute the residual stress intensity factor, however, this method presents uncoherent results when compared with experimental data, as it can be observed. On the other hand, if the elementary block size is computed with Eq. (3), results can be correlated with experimental evidences. The computation of the predicted FCG for both methods were based on the results described in Table 6.

6. Conclusions

A unified two-stage fatigue methodology was implemented to assess the fatigue crack propagation behaviour of S355 considering the plasticity induced crack closure effect. The cyclic elastoplastic behaviour of this material was assessed by analysing experimental data from previous researches. Low-cycle fatigue behaviour was determined using the Smith-Watson-Topper fatigue damage parameter. Fatigue crack growth tests were performed on CT specimens using different values for stress ratio. It was evident that fatigue crack growth of S355 is influenced by the mean stress effect. The effective value of the stress intensity factor was computed during FCG tests using Elber concept showing a converge in a uniform trend of the fatigue crack growth rate.

UniGrow model was implemented to analyse fatigue crack growth behaviour of this material. The first step was to compute the residual stresses ahead of the crack tip induced by the load reversal and determine the value of the crack tip radius that better correlates with experimental results. It was found that crack tip radius should be $\rho = 3.4E^{-6}m$ since it is the value that leads to lower mean squared error. The smaller the value of the crack tip radius, the closer we are to the experimental values, but the value proposed in this paper is the one that leads to satisfactory results by comparing with experimental data and to adequate process time. A numerical model was also implemented using the value of the crack tip radius proposed in which the main goal was to validate the residual compressive stress field ahead of the crack tip. Comparison between experimental, numerical and analytical approaches showed a good agreement in what concerns residual stress intensity factor.

Finally, fatigue crack growth rates were computed using different approaches for the elementary block size. As it is proposed in original UniGrow model, the elementary block size used to collapse FCG data is the same as the crack tip radius used to compute residual stresses ahead of the crack tip. However, it is evident from the results that if this approach is implemented, there is no good correlation with experimental FCG data. The proposal in this paper is to relate the elementary block size with the crack tip plasticity by establishing a relation between elementary block size and effective stress intensity factor and cyclic yield strength of the material. Since monotonic and cyclic crack tip plasticity increases during the FCG test, it is expected that elementary block size also varies and a new expression was proposed by correlation with experimental FCG data.

Future investigations should be focused on finding different approaches to compute the stress–strain field ahead of the crack tip, namely by considering digital image correlation, in order to further validate the expression proposed for elementary block size. Other types of metallic materials should also be studied in order to analyse the possible generalization of the proposed approach.

Declaration of Competing Interest

The authors declare that they have no known competing financial interests or personal relationships that could have appeared to influence the work reported in this paper.

Acknowledgements

The authors would like to acknowledge the Fundação para a Ciência e Tecnologia (FCT) for funding the PhD scholarship SFRH/BD/145037/2019. Additionally, this research was also supported by the following grants: project grant (POCI-01-0145-FEDER-030103) FiberBridge - Fatigue strengthening and assessment of railway metallic bridges using fiber-reinforced polymers by national funds (PIDDAC) through the Fundação para a Ciência e Tecnologia (FCT/MCTES); base funding - UIDB/04708/2020 and programmatic funding - UIDP/04708/2020 of the CONSTRUCT - Instituto de I&D em Estruturas e Construções - funded by national funds through the FCT/MCTES (PIDDAC); AARM4 - High Strength Steels in Metalmechanics 4.0 (POCI-01-0247-FEDER-068492) funded by national funds through the PT2020/COMPETE; and, individual project grant (2020.03856.CEECIND), awarded to José A.F.O. Correia, by national funds (PIDDAC) through the Fundação para a Ciência e Tecnologia (FCT/MCTES).

References

[1] Paris P, Erdogan F. A critical analysis of crack propagation laws. J Basic Eng 1963;85(4):528–33.
[2] Wolf E. Fatigue crack closure under cyclic tension. Eng Fract Mech 1970;2(1):37–45.
[3] Glinka G. A notch stress-strain analysis approach to fatigue crack growth. Eng Fract Mech 1985;21(2):245–61.
[4] Peeker E, Niemi E. Fatigue crack propagation model based on a local strain approach. J Constr Steel Res 1999;49(2):139–55.
[5] Noroozi A, Glinka G, Lambert S. A two parameter driving force for fatigue crack growth analysis. Int J Fatigue 2005;27(10-12):1277–96.
[6] Noroozi A, Glinka G, Lambert S. A study of the stress ratio effects on fatigue crack growth using the unified two-parameter fatigue crack growth driving force. Int J Fatigue 2007;29(9-11):1616–33.
[7] Noroozi AH, Glinka G, Lambert S. Prediction of fatigue crack growth under constant amplitude loading and a single overload based on elasto-plastic crack tip stresses and strains. Eng Fract Mech 2008;75(2):188–206.
[8] Hurley PJ, Evans WJ. A methodology for predicting fatigue crack propagation rates in titanium based on damage accumulation. Scr Mater 2007;56(8):681–4.
[9] Ferreira SE, Castro JTPd, Meggiolaro MA. Using the strip-yield mechanics to model fatigue crack growth by damage accumulation ahead of the crack tip. Int J Fatigue 2017;103:557–75.
[10] Correia JAFO, de Jesus AMP, Fernández-Canteli A. A procedure to derive probabilistic fatigue crack propagation data. Int J Struct Integr 2012;3(2):158–83.
[11] Hadi Hafezi M, Nik Abdullah N, Correia JFO, De Jesus AMP. An assessment of a strain-life approach for fatigue crack growth. vol. 3. 2012. /10.1108/17579861211281173.
[12] Jesus A, Correia J. Critical assessment of a local strain-based fatigue crack growth model using experimental data available for P355NL1 steel. J Press Vessel Technol 2013:135.

[13] Correia JAFO, de Jesus AMP, Fernández-Canteli A, Calçada RAB. Modelling probabilistic fatigue crack propagation rates for a mild structural steel. Frat Ed Integrita Strutt 2015;31:80–96. https://doi.org/10.3221/IGF-ESIS.31.07.
[14] Bogdanov S, Mikheevskiy S, Glinka G. Probabilistic analysis of the fatigue crack growth based on the application of the monte-carlo method to unigrow model. Mater Perform Charact 2014;3:20130066. https://doi.org/10.1520/MPC20130066.
[15] Correia JAFO, De Jesus AMP, Fernández-Canteli A. Local unified probabilistic model for fatigue crack initiation and propagation: Application to a notched geometry. Eng Struct 2013;52:394–407.
[16] Correia J, Apetre N, Arcari A, De Jesus A, Muñiz-Calvente M, Calçada R, et al. Generalized probabilistic model allowing for various fatigue damage variables. Int J Fatigue 2017;100:187–94.
[17] Bang DJ, Ince A, Tang LQ. A modification of UniGrow 2-parameter driving force model for short fatigue crack growth. Fatigue Fract Eng Mater Struct 2019;42(1):45–60.
[18] Bang DJ, Ince A, Noban M. Modeling approach for a unified crack growth model in short and long fatigue crack regimes. Int J Fatigue 2019;128:105182.
[19] Bang DJ, Ince A. A short and long crack growth model based on 2-parameter driving force and crack growth thresholds. Int J Fatigue 2020;141:105870.
[20] Kujawski D. An estimation of elastic–plastic strain and stress ahead of a fatigue crack in Mode I. Theor Appl Fract Mech 2021;115:103070.
[21] Kujawski D. A damaging function ΔKd for analyzing FCG and R-ratios in metallic materials. Theor Appl Fract Mech 2021;116:103091.
[22] Kujawski D. Correlating R-ratio effects on FCG behavior using ΔKd function. Theor Appl Fract Mech 2022;118:103244.
[23] Mikheevskiy S, Bogdanov S, Glinka G. Analysis of fatigue crack growth under spectrum loading – The UniGrow fatigue crack growth model. Theor Appl Fract Mech 2015;79:25–33.
[24] Irwin G. Analysis of stresses and strains near the end of a crack traversing a plane. J Appl Mech 1957;24:361–4.
[25] Hutchinson JW. Singular behaviour at the end of a tensile crack in a hardening material. J Mech Phys Solids 1968;16(1):13–31.
[26] Lal DN, Weiss V. A notch analysis of fracture approach to fatigue crack propagation. Metall Trans A 1978;9(3):413–26.
[27] Neuber H. Theory of stress concentration for shear-strain prismatic bodies with arbitrary nonlinear stress-strain law. J Appl Mech 1961;28:544–50.
[28] Creager M, Paris PC. Elastic field equations for blunt cracks with reference to stress corrosion cracking. Int J Fract Mech 1967;3(4):247–52.
[29] Moftakhar A, Buczynski A, Glinka G. Calculations of elasto-plastic strains and stresses in notches under multiaxial loading. Int J Fract 1995;70:357–73.
[30] de Jesus AMP, Matos R, Fontoura BFC, Rebelo C, Simões da Silva L, Veljkovic M. A comparison of the fatigue behavior between S355 and S690 steel grades. J Constr Steel Res 2012;79:140–50.
[31] Carvalho D. Comportamento à fadiga de aços estruturais. MSc Thesis, Universidade de Trás-os-Montes e Alto Douro 2014.
[32] ASTM E 606. Standard Practice for Strain Controlled Fatigue Testing. Annual Book of ASTM Standards: American Society for Testing and Materials; 1998.
[33] Smith K, Watson P, Topper T. A stress-strain function for the fatigue of metals. J Mater 1970;5:767–78.
[34] ASTM E 647. Standard Test Method for Measurement of Fatigue Crack Growth Rates. American Society for Testing and Materials; 2015.
[35] Hibbit D, Karlsson B, Sorensen P. ABAQUS/Standard User's Manual, Ver. 6.10. Pawtucket, Rhode Island: 2004.